Journal of Power Sources 225 (2013) 356–363

Contents lists available at SciVerse ScienceDirect

Journal of Power Sources

journal homepage: www.elsevier.com/locate/jpowsour

# A new method for manufacturing graphene and electrochemical characteristic of graphene-supported Pt nanoparticles in methanol oxidation

Karim Kakaei [a,*], Mohammad Zhiani [b]

[a] Department of Chemistry, Faculty of Science, University of Maragheh, 55181-83111 Maragheh, Iran
[b] Department of Chemistry, Isfahan University of Technology, 84156-83111 Isfahan, Iran

## HIGHLIGHTS

- Graphene is electrosynthesised.
- Pt/Gr is prepared.
- Methanol OX activity was 1315 $Ag^{-1}$ Pt.

## ARTICLE INFO

*Article history:*
Received 20 June 2012
Received in revised form
22 August 2012
Accepted 1 October 2012
Available online 26 October 2012

*Keywords:*
Electrochemical exfoliation
Graphene
Platinum nanoparticles
Methanol oxidation

## ABSTRACT

We report a Pt/graphene catalyst for the methanol oxidation. Graphene is synthesized from graphite electrodes using ionic liquid-assisted electrochemical exfoliation. Graphene-supported Pt electrocatalyst is then reduced by sodium borohydride with ethylenediaminetetraacetic acid disodium salt (EDTA-2Na) as a stabilizing agent to prepare highly dispersed Pt nanoparticles on carbon graphene to use as methanol oxidation in direct methanol fuel cell (DMFC) catalysts. X-ray diffractometer and scanning electron microscopy technique are used to investigate the crystallite size and the surface morphologies respectively. The electrochemical characteristics of the Pt/graphene and commercial Pt/C catalysts are investigated by cyclic voltammetry (CV) in nitrogen saturated sulfuric acid aqueous solutions and in mixed sulfuric acid and methanol aqueous solutions. The catalytic activities of the Pt/graphene and Pt/C electrodes for methanol oxidation is 1315 A $g^{-1}$ Pt and 725 A $g^{-1}$ Pt, which can be revealed the particular properties of the exfoliated graphene supports. Furthermore, Pt/graphene exhibited a better sensitivity, signal-to-noise ratio, and stability than commercial Pt/C.



## 1. Introduction

Direct methanol fuel cells (DMFCs) are considered one of the most promising power sources for applications in electric vehicles and electronic portable devices, due to their high power density, relatively quick startup, rapid response to varying loading, and low operating temperature [1–3].

The use of methanol as fuel has several advantages in comparison to hydrogen: it is a cheap liquid fuel, easily handled, transported, stored, and with a high theoretical energy density [4–6].

The major problem in the development of DMFC is the poor kinetic of the anode reaction [6] which leads to high overpotentials. To overcoming of kinetic problems there are several attempts have been done by researchers [7,8].

In one of the methods, the Pt catalyst surface is modified by the addition of a second metal [9], but this approach is not affordable. The other strategy is to develop new catalyst supports with the aim of increasing the catalysts' dispersion, utilization, activity, and stability [10]. Carbon comes in many different forms, and now scientists have predicted another new form, or allotrope, of carbon. One currently popular carbon support is Vulcan XC-72 carbon black. However, the rate of methanol electrooxidation on this conventional carbon support is low, partly due to low platinum utilization, which is, in turn, related to the small electrochemically accessible surface area that is available for the deposition of Pt particles [10]. The other carbon support uses in catalyst support is carbon nanotube, but not cost effective. The new form of carbon, which they call graphene, has very intriguing physical properties that suggest it could have a wide variety of applications. Graphene has received significant attention in recent years due to their unique electronic, physical, mechanical, thermal and chemical properties, such as high surface area, excellent conductivity, ease of

* Corresponding author. Tel.: +98 421 2276068; fax: +98 421 2276066.
*E-mail addresses:* kakaei@maragheh.ac.ir, k_kakaei56@yahoo.com (K. Kakaei).

0378-7753/$ – see front matter © 2012 Elsevier B.V. All rights reserved.
http://dx.doi.org/10.1016/j.jpowsour.2012.10.003

functionalization and potentially low manufacturing cost since their discovery in 2004 [11,12]. Graphene provides an ideal base for electronics, energy storage devices, sensors [13,14] transparent electrodes [15,16], supercapacitor [17], and methanol oxidation [18–26].

Li et al. [18] investigated the catalytic performance of Pt nanoparticles on reduced graphene oxide for methanol electrooxidation. Li et al. [19] prepared and characterized the electrochemical performance of Pt/graphene nanocomposites for methanol oxidation. Bong et al. [20] used of graphene supported electrocatalysts in DMFC. However, in all of these papers graphene was synthesized by chemical method and the electrochemical characteristic was not studied carefully. The chemical methods cannot be produced in large-scale graphene and toxic substances used in its construction (Hummers method) [27]. In addition in this paper we used of urea choline chloride as an ionic liquid in order to synthesis of graphene nanosheets by electrochemical method and is used as the basis of platinum nanoparticles. The mechanism of the exfoliation of carbon graphite in ionic liquid is described by Lu et al. [28]. So, graphene-supported Pt nanoparticles with 10 wt. % metal loading are prepared by sodium borohydride reduction method and the electrochemical characteristic of Pt/graphene is studied carefully and compared with commercial Pt/C (E-TEK) under methanol oxidation.

## 2. Experimental

### 2.1. Graphene preparation

The graphite rod was inserted as anode into the ionic liquid (IL)/water solution, placed parallel to the Pt wire as counter-electrode with a separation of 1 cm the ionic liquid Urea choline chloride was mixed with water at 1:1 ratio. Static potentials of 5 V were applied to the two electrodes using a DC power supply. The exfoliation products were washed with water and surfactant until the pH was neutral and the products were separated by filter and ultra centrifugation at 10,000 rmp at 25 °C. Three stages in the electrochemical exfoliation, which represent the beginning of electrochemical reaction and the end of reaction in the process of electrochemical oxidation, intercalation, and corrosion of the graphite anode, are occurred. In stage I, there is an induction period before visible signs of exfoliation can be detected. The color of the electrolyte changed from colorless to yellow and then dark brown. In stage II, a visible corrosion and expansion of the graphite anode can be seen. In stage III, the expanded flakes peel off from the anodes and form the black slurry with the electrolyte [28].

### 2.2. Preparation of Pt/graphene

The synthesis of Pt nanoparticles dispersed onto graphene (Pt/graphene) was carried out by chemical reduction of platinum on to graphene oxide (GO). It is noted that, graphene oxide could be reduced by different agent such as, glucose [29], hydrazine [30], borohydride [31] and so on. Furthermore $Pt^{+4}$ capability to be reduced by borohydride [32] ethylene glycol [33] and so on.

In this reaction system for the synthesis of Pt/graphene, borohydride not only could be reduced the remaining graphene oxide to graphene, but also could be reduced $Pt^{+4}$ in the water. On the other hand, in the reaction system for preparation of Pt/graphene nanocomposites, borohydride could be acted as reducing agent for reduction of Pt nanoparticles from their precursors and reduction of graphene from the remaining graphene oxide.

For synthesizing the Pt/graphene with EDTA-2Na/Pt ratios of 1:1, the corresponding 0.08744 g of EDTA-2Na in 5 ml of water was added to 1.326 ml of $3.86 \times 10^{-2}$ M $H_2PtCl_6 + 6H_2O$ in water. Then the PH value of the mixture was adjusted to 7–8 by aqueous NaOH solution (0.1 M) under vigorous stirring. Then the obtained yellow solution was mixed with the graphene (200 mg) in 66.3 ml of water/methanol (1:1) solution homogeneously, followed by sonicated for 60 min. Finally borohydride/water solution (50 ml, 37%) was added drop by drop. The resulting mixture was stirred at 73 °C for 24 h until colorless. During the reaction process, the pH value of the system must be maintained within 7–8 by addition of a NaOH aqueous solution (0.1 M). And so, the products were filtered, washed with excess deionized water, then dried at 90 °C. A Pt/graphene catalyst with EDTA-2Na/Pt ratio of 1:1 was also treated with a similar procedure for comparison purposes. The Pt content was determined by ICP to be 10% Pt.

### 2.3. Ink preparation

A mixture containing a homogeneous suspension of commercially available Pt catalyst powder (Pt/C 10 wt. %) Inc. as a reference material catalyst. Isopropanol (Merck), water, 10 wt % Nafion solution and reference material catalyst were homogenized by sonication for 20 min, and then painted onto glassy carbon electrode. The resulting composite structure was dried in air at 100 °C for 2 h and denoted as Pt/C (E-TEK) electrode [34]. The second electrode was manufactured by above procedure and mixed with isopropanol (Merck), water, 10 wt % and Nafion solutions then were homogenized by sonication for 20 min and denoted as Pt/graphene electrode.

### 2.4. Electrochemical measurements

All the electrochemical experiments were performed with a conventional three compartment electrolytic cell with a water jacket for maintaining stable temperature conditions in the electrolyte and μAUTOLAB Type III Potentiostat–Galvanostat with computerized control by GPES (General Purpose Electrochemical Software) software. A Pt rod of 3.1 $cm^2$ apparent area was used as the auxiliary electrode and a double junction Ag|AgCl|KCl (saturated) electrode was employed as the reference electrode. All potentials given in this work are referred to the reversible hydrogen electrode (RHE) in the working electrolyte electrode. A glassy carbon disk held in a Teflon cylinder with a geometrical surface area of 0.031415 $cm^2$ was used as working electrode. The electrolyte was firstly deaerated by bubbling $N_2$ for 30 min.

## 3. Results and discussion

### 3.1. Characterization of Pt/graphene and Pt/C electrodes

Scanning electron microscopy (SEM) micrographs of the prepared electrodes are shown in Figs.1 and 2. The surface of the Pt/C electrode was rough and porous. A comparison of the images revealed that the morphology of the Pt/C electrode was significantly more homogeneous, and the platinum nanoparticles were not visible (Fig. 1). However, the morphology of the Pt/graphene electrode was different. SEM analysis of Fig. 2 revealed the presence of large, transparent graphene sheets with few layers. Platinum particles are too small to detect at the maximum resolution attainable with the microscope.

Fig. 3 illustrates the X-ray diffraction (XRD) patterns of graphene and Pt/graphene composite. The characteristic diffraction peaks of graphene (Fig. 3a) at 24.2° is ascribed to the introduction of oxygenated functional groups, such as epoxy, hydroxyl (–OH), carboxyl (–COOH) and carbonyl (–C]O) groups attached on both sides and edges of carbon sheets. These surface functional groups will subsequently act as anchoring sites for metal complexes [35].

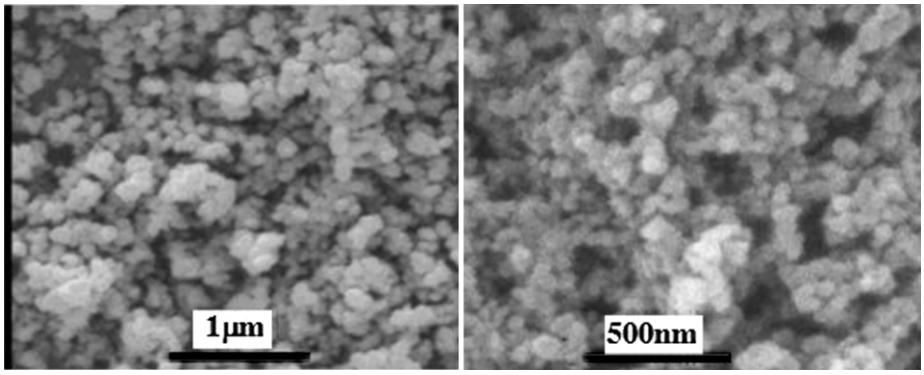


**Fig. 1.** SEM micrographs of the surface of the Pt/C electrode, recorded at 15,000× and 30,000× magnification.

The diffraction peak at around 43° is associated with the (100) plane of the hexagonal structure of carbon [36].

Fig. 3b shows X-ray diffractions of Pt/graphene catalyst. The strong diffraction peaks at $2\theta = 39.9°$, 46.3°, 68.2° and 81.4° can be assigned to the characteristic (111), (200), (220) and (311) crystalline planes of Pt, respectively, which possesses face-centered-cubic (fcc) structure. The XRD patterns of graphene and graphene–platinum nanoparticle composite, indicating that the graphene structure was not destroyed after the in situ chemical reduction.

It is well known that graphene can be chemically converted from GO by removing the surface functional groups using physical or chemical reduction [37,38]. However, electrochemical method is an effective tool to modify electronic states via adjusting the external power source to change the Fermi energy level of electrode materials surface, electrochemical reduction of the exfoliated GO on graphite electrode or use of ionic liquids for the electrochemical exfoliation of graphite.

Average Pt crystallite size is frequently calculated from XRD peak broadening using the Scherrer equation [34] for the (111) peak, yielding value of 4.8 nm for the Pt/graphene catalysts.

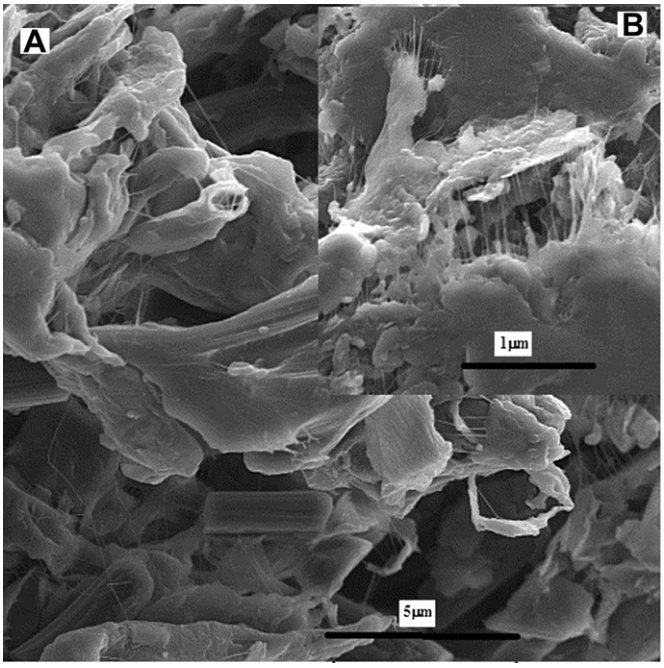


**Fig. 2.** SEM micrograph of the surface of the Pt/graphene electrode recorded at 5000 and 15,000× magnification.

### 3.2. Electrochemical active surface area and roughness factor

The electrochemical behaviors of the Pt/C and Pt/graphene were investigated with CV: at low potentials, between −0.03 and +0.15 V (vs. RHE), the typical peaks are related to hydrogen adsorption/desorption and both the anodic and cathodic currents show the presence of Pt particles (Fig. 4). The ECSAs of these electrodes were calculated by using the columbic charge for hydrogen desorption [39].

The ECSA of Pt/graphene electrode calculated from the voltammogram is higher than that of Pt/C electrode. It should be noted that the value of double layer is corrected. The calculated values for both electrodes are listed in Table 1.

Moreover, the platinum deposits were characterized by calculating the following parameters such as the true surface ($S_{true}$, $cm^2$), the specific surface ($S_{sp}$) or ECSA ($S_{sp} = S_{tru}/m_{Pt}$, $m^2\ g^{-1}$), the roughness factor ($\Gamma = S_{true}/S_{geom}$), and the platinum loadings ($m_{Pt}$, μg) [40,41].

The electrocatalytic activities of these electrodes depend on the roughness factor (the ratio between the real surface area and the geometrical area of electrode) and the existence of special binding sites on the surface of the particles [42]. Low roughness and slow electron transport limit their catalytic performance. Compared with the commercial Pt/C electrode, the Pt/graphene electrode with nanoporous structure possessed much higher roughness (Table 2) and better electron transport, which led to distinguished performance in the methanol oxidation.

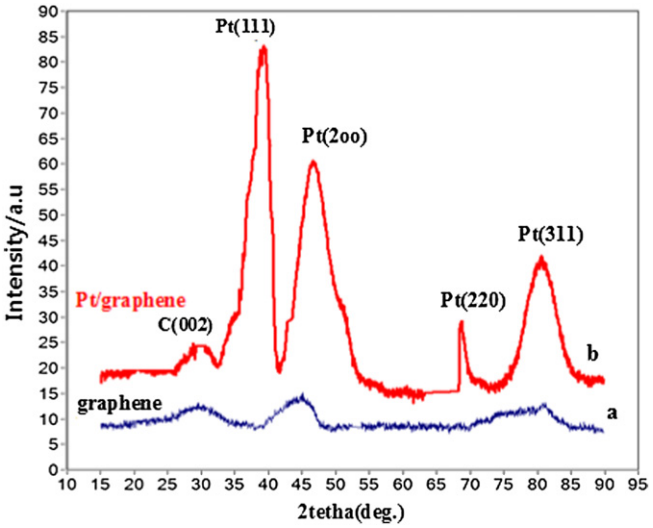


**Fig. 3.** XRD patterns of (a) graphene and (b) Pt/graphene.

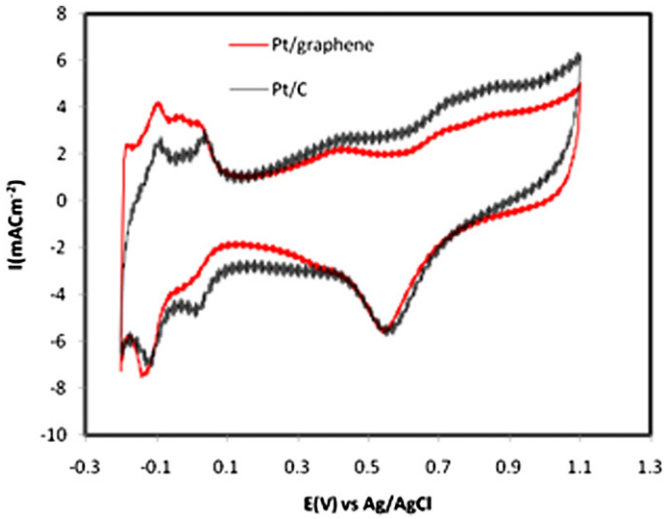


**Fig. 4.** Cyclic voltammograms of the Pt/C and Pt/graphene catalysts in 0.5 M $H_2SO_4$ electrolyte solution, collected at a scan rate of 50 mV $s^{1}$ at room temperature.

### 3.3. CVs for methanol electrooxidation

Before the methanol oxidation analyses, the prepared electrodes were activated by CV at a scan rate of 50 mV $s^{-1}$ with applied potentials ranging from −0.03 to 1.297 V vs, RHE for 100 cycles in nitrogen saturated 0.5 M $H_2SO_4$ aqueous solution.

Fig. 5 shows the CVs for methanol oxidation on the Pt/C and Pt/graphene electrodes. A comparison of Figs. 4 and 5a reveals that the onset potentials for methanol oxidation on the Pt/graphene was 180 mV and significantly lower than the onset potentials at the Pt/C catalysts, measured to be 280 mV. The measured onset potential for the Pt/graphene electrode was very close to that of the Pt–Ru catalyst, which yields an onset potential of 150 mV. The CV analyses for evaluating methanol oxidation efficiency of the electrodes were performed at a scan rate of 50 mV $s^{-1}$ with potentials ranging from −0.03 to 1.297 V vs, RHE for 100 cycles. The voltammograms of each electrode became stable and similar after the hundredth cycle. All electrochemical characteristic data of the tests are summarized in Table 1. Fig. 5a shows the results from the hundredth cycle. The voltammogram of Pt/graphene was distinctly different from that obtained on Pt/C electrode. The electrode activities on methanol oxidation were compared in items of forward peak current density, a ratio of the forward peak current density ($i_f$) to the backward peak current density ($i_b$), and the mass activity (MA, peak current density of methanol oxidation obtained from CV per unit Pt loading mass

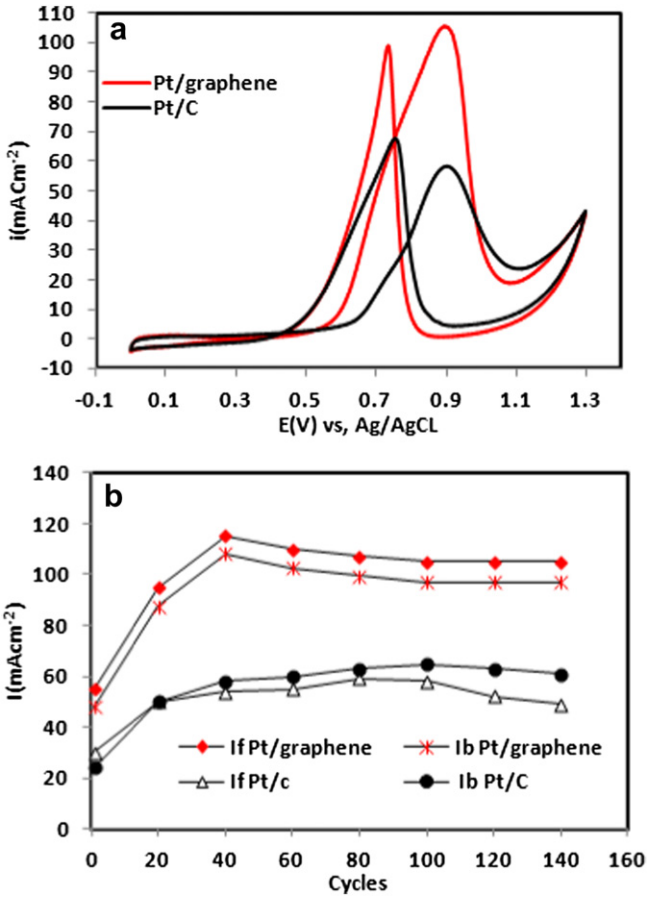


**Fig. 5.** (a) Cyclic voltammograms of the Pt/C and Pt/graphene electrodes with a Pt loading level of 80 μg $cm^{-2}$ in 1 M $CH_3OH$ + 0.5 M $H_2SO_4$ collected at a sweep rate of 50 mV $s^{-1}$. CVs were obtained after 100 cycles. (b) Cycling performance of electrocatalysts for the methanol oxidation.

[43]), as mentioned in Table 1. During the forward scan, methanol is oxidized and the surface of the Pt will be covered by poisonous materials, such as carbon monoxide et al. under the potential of 0.5–0.9 V vs. RHE, and then the current decreases due to the deactivation of the Pt surface. The poisonous materials would be oxidized at such high potential like 0.9 V vs. RHE. But since the Pt surface is covered with Pt oxide under such high potential, the activity of methanol oxidation will decrease or disappear. In the reverse scan, there are no poisonous materials on the surface. The big oxidation current would

**Table 1**
Catalyst loadingas and electrochemical characteristics of the samples during CV and noise analyses.

| Samples | Loading Pt (μg $cm^{-2}$) | $V_p$ (vs. RHE) | $i_P$ (mA $cm^{-2}$) | $i_f/i_b$ | Mass activity (A $g^{-1}$ Pt) | $E_{onst}$ (vs. RHE) | ECASA ($m^2$ $g^{-1}$) | S/N |
|---|---|---|---|---|---|---|---|---|
| Pt/C | 80 | 0.907 | 58 | 0.865 | 725 | 0.477 | 25.2 | 4.16 |
| Pt/graphene | 80 | 0.898 | 105.23 | 1.071 | 1315.375 | 0.377 | 38.3 | 5.9 |

**Table 2**
Roughness factors of Pt/C and Pt/graphene catalysts on GC substrate in 0.5 M $H_2SO_4$ recorded at 50 mV $s^{-1}$ and kinetic parameters for methanol oxidation on Pt/C and Pt/graphene electrocatalyst.

| Sampels | $S_{true}$ ($cm^2$) | $S_{sp}$ ($m^2$ $g^{-1}$) | $S_{geometric}$ ($cm^2$) | Raghness factor ($\Gamma$) | $b$ (mV $dec^{-1}$) | $\alpha$ | $i_0$ |
|---|---|---|---|---|---|---|---|
| Pt/C | 0.633024 | 25.2 | 0.031415 | 20.16 | 76 | 0.4 | $1.47 \times 10^{-7}$ |
| Pt/graphene | 0.962096 | 38.3 | 0.031415 | 30.64 | 62 | 0.52 | $3.1 \times 10^{-6}$ |

be due to the methanol oxidation, not by the desorption of poisonous materials. Pt oxide formed during forward scan is reduced at lower potential than 0.6 V and the Pt surface is covered with clean surface. The result was consistent with the relatively higher $i_f/i_b$ values of Pt/graphene, as also listed in Table 1, highlighting a more efficient CO desorption on this electrode.

Fig. 5b shows the changes in $i_f$ and $i_b$ values as a function of cyclic voltammogram. The study was performed over 140 cycles. In the cycle 40 for the Pt/C, it was observed that the current density peak from $i_b$ is already higher than $i_f$ peak; this result indicates that commercial Pt/C has affinity with the adsorbed species and it is a limiting process for an adequate anodic electro-catalyst. In the case of Pt/graphene electrode, during the 140 cycles, $i_f/i_b$ ratio remained almost constant, indicating the long-term activity of the synthesized Pt/graphene in comparison to Pt/C to catalyze the methanol oxidation reaction.

In order to further investigate the effect of graphene on methanol oxidation efficiency, calculated mass activity (MA) data were also examined. It was marked that the MA value of Pt/graphene was 1.81 times greater than that of Pt/C electrode, indicating that the Pt/graphene electrode shows higher activity for methanol oxidation than that for Pt/C electrode.

### 3.3.1. Effect of the scan rate in cyclic voltammetry

Fig. 6 shows the CVs recorded for methanol oxidation on Pt/C in 0.50 M $H_2SO_4$ + 1.00 M $CH_3OH$ at scan rates between 2 and 80 mV $s^{-1}$. The increase in peak current with the scan rate can be analyzed considering an adsorption or diffusion control of the reaction. While for an irreversible process controlled by adsorption, the Ep–$\nu$ and Ip–$\nu$ relationships are given by Cabot et al. [44] for diffusion control.

A slope of 1.0 or 0.5 is then expected for the log Ip–log $\nu$ plots under adsorption or diffusion control, respectively. Using the dependency of anodic peak potential on the logarithm of the sweep rate (Fig. 6c), the value of $\alpha$ was obtained as 0.1782. A possible explanation for this behavior is the existence of a kinetic contribution to the reaction control, as expected if the charge transfer for the methanol oxidation on Pt/C is considerably slow in the studied potential range taking place a mixed (diffusion-kinetic or adsorption-kinetic) control. For this reason, the apparent Tafel slope of 43.4 mV $dec^{-1}$ obtained for the linear Ep–log $\nu$ plot shown in Fig. 7b, due to the much lower value of 0.1782 (Fig. 6c) and mixed diffusion-kinetic control, cannot be applied to calculate the kinetic parameters for the methanol oxidation. However, in the case of Pt/graphene the Tafel slope of 53.5 mV $dec^{-1}$ obtained for the linear Ep–log $\nu$ plot shown in Fig. 7b because of the value of $\alpha$ close to 0.5 (Fig. 7c) can be used to estimate the kinetic parameters.

### 3.3.2. Tafel slope and exchange current density

The kinetic analysis for the oxidation of methanol on the Pt/graphene and Pt/C electrodes was made considering the classical $E$ vs. log $I$ plot, provided in Fig. 8. The Pt/graphene electrode has a better performance in the region under kinetic control compared with the commercial Pt/C electrode. Excellent linear correlations are found between 0.4508 and 0.607 V in each case, and Table 2 collects the corresponding Tafel slopes (b) thus obtained. Pt/graphene present Tafel slopes very close to the Ep–log $\nu$ value of 53.5 mV $dec^{-1}$. However, in the case of Pt/C, this parameter offers

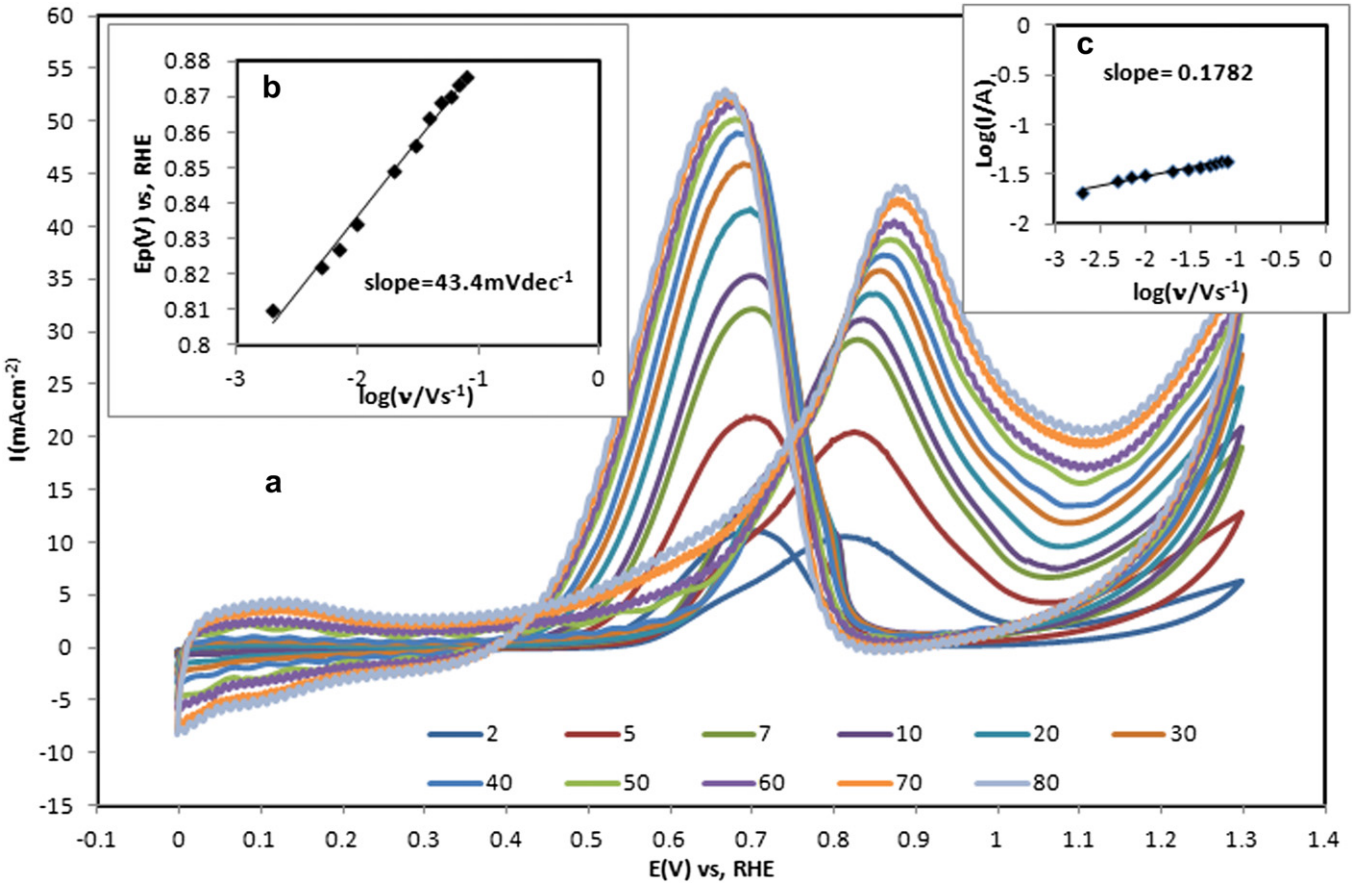


**Fig. 6.** (a) CV curves of 1 mol methanol in 0.5 mol $H_2SO_4$ solution on the Pt/C electrode at scan rates between 2 and 80 mV $s^{-1}$, and 25.0 °C. (b) Log of peak current and (c) peak potential vs. log of scan rate for the methanol oxidation from the voltammograms.

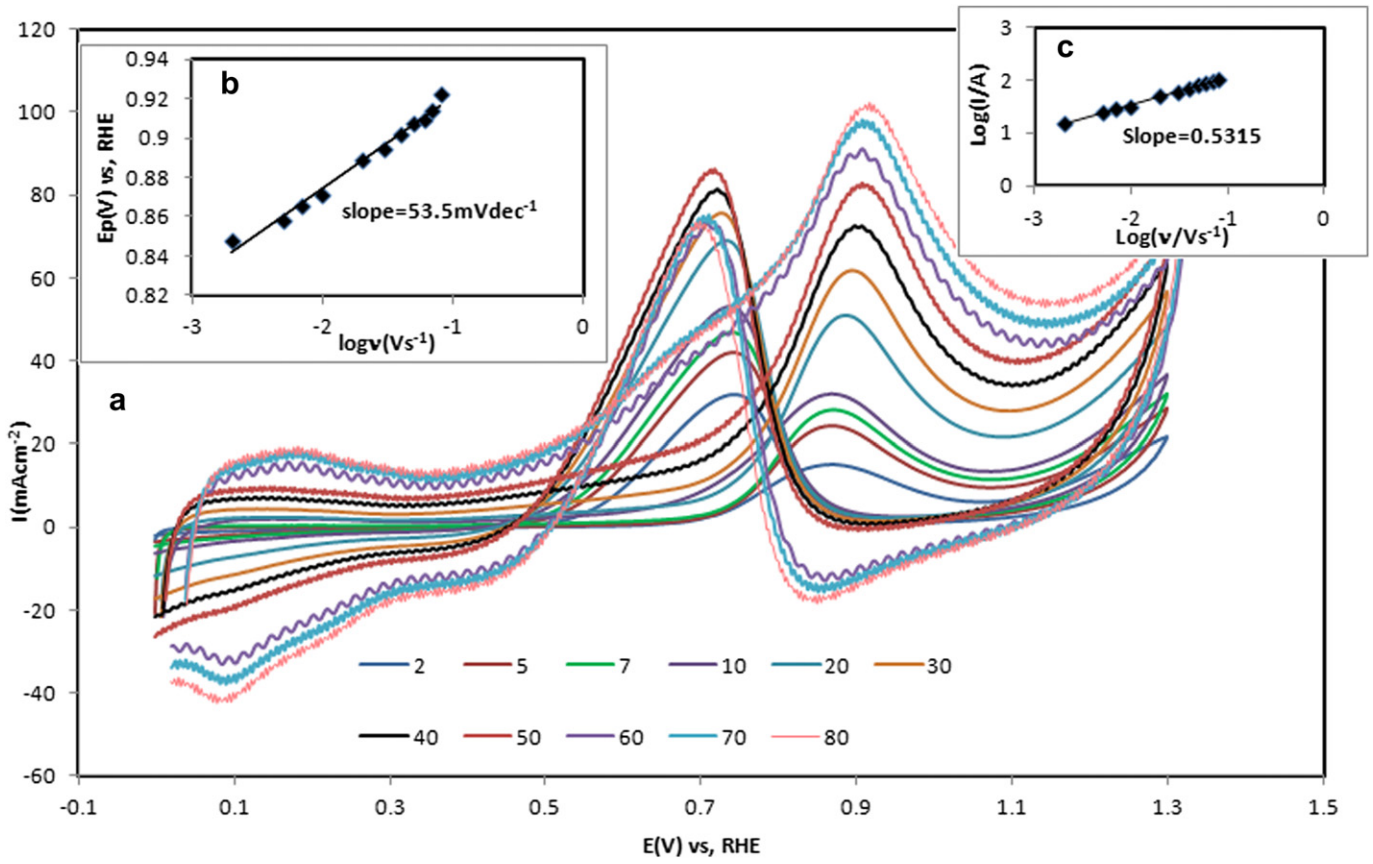


**Fig. 7.** (a) CV curves of 1 mol methanol in 0.5 mol $H_2SO_4$ solution on the Pt/graphene electrode at scan rates between 2 and 80 mV $s^{-1}$, and 25.0 °C. (b) Log of peak current and (c) peak potential vs. log of scan rate for the methanol oxidation from the voltammograms.

a higher value, 72 mV $dec^{-1}$ ($\alpha = 0.45$). In the literature, the Tafel slope for methanol oxidation on Pt varies from 60 mV $dec^{-1}$, using Pt single crystals covered by spontaneously deposited Ru at room temperature [45], 123 mV $dec^{-1}$ for Pt/C at 20 mV $s^{-1}$ [44] to 195 mV $dec^{-1}$ at 60 °C with bulk Pt–Ru alloy [46], obviously indicating that this parameter is strongly dependent on the catalyst morphology and the experimental conditions. The exchange currents ($i_0$) for methanol oxidation were then estimated by extrapolating the Tafel plots of Fig. 8 to the standard potential of the reaction (0.046 V), based on Butler–Volmer approach, and its normalization by the geometrical electrode area yielded the corresponding exchange current densities ($i_0$, MeOH). These data are given in Table 2, where the exchange current density of Pt/graphene electrode calculated from the linear sweep voltammetry is higher than that of Pt/C electrode.

### 3.4. Comparison of stability and signal-to-noise ratio of Pt/graphene and Pt/C

We also estimated the stability of the Pt/graphene electrode by performing chronoamperometry scans in methanol aqueous. In order to compare, the same set of experiments was also performed using Pt/C. However, it was interesting that the observed decrease in the current density was measured to be 44% for Pt/graphene in the 900 s and the corresponding decrease for the Pt/C electrode was found to be 67% (Fig. 9). This demonstrated that graphene could reduce the CO poisoning and enhance the activity and stability of the Pt incorporated into the graphene relative to Pt reduced onto the Vulcan XC-72 substrate. All the above behavior can be attributed to the presence of larger density of $sp^2$ planes (resulted as a consequence of reduction of graphitic oxide to yield graphene) that favors methanol oxidation electrochemistry [47].

Moreover, we also evaluated the signal-to-noise (S/N) response of the Pt/Graphene (Fig. 10) and Pt/C (Fig. 11) in 1 M $CH_3OH$ + 0.5 M $H_2SO_4$. The working electrode's size, shape, and material undoubtedly influence the signal and the noise obtained [48]. Electrochemical Noise is a nondestructive technique to reflect the individual sum of random events of potential fluctuations and/or current of a material subject to corrosive conditions and the value of the Root Mean Square (RMS) of amplitude of these events or standard deviation has been providing the fingerprint of the amount of dissolved metal, depending on the metal–environment combination [49]. On the other hand, as the dimension and the operating voltage of modern electronic devices are reduced, its low-frequency noise is becoming a critical parameter determining the device performance. Especially, $1/f$ noise can be a significant problem in the devices based on nanomaterials such as graphene, carbon nanotubes and nanowires [50]. Furthermore, the nanoscale noise map of a graphene strip was successfully obtained by Sung et al. [50], which allowed to study the effect of structural defect on the noise in graphene strip channel. Electrochemical noise data were recorded using a μAUTOLAB Type III Potentiostat–Galvanostat and GPES (General Purpose Electrochemical Software) software. To estimate the S/N Pt/Graphene or Pt/C electrodes, we initially evaluated their noise (N) by performing chronoamperometry of the electrodes in $H_2SO_4$. In a similar way, their corresponding

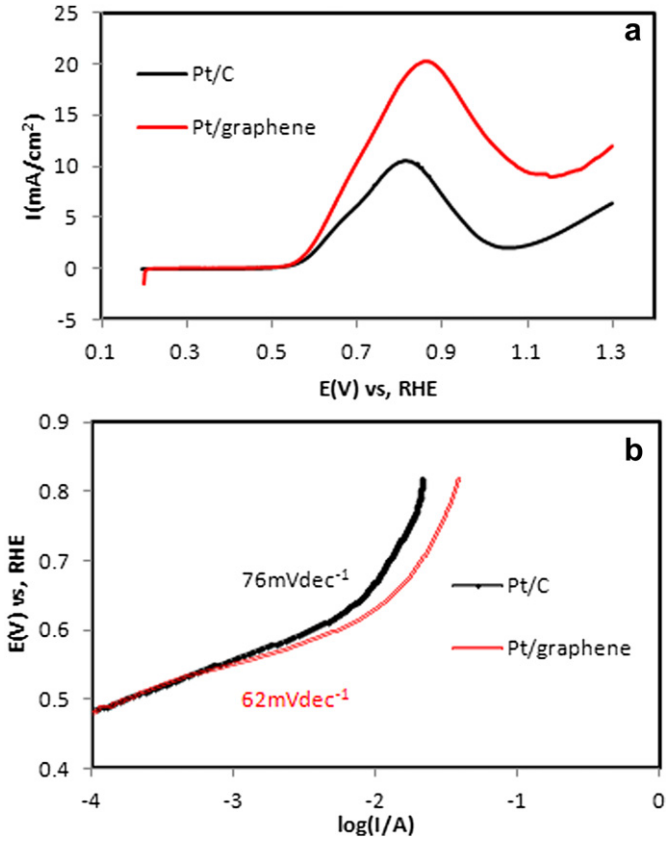


**Fig. 8.** (a) Linear sweep voltammetry for methanol oxidation on Pt/C and Pt/graphene electrodes in 1 M $CH_3OH$ + 0.5 M $H_2SO_4$ at 25.0 °C. Sweep rate 1 mV $s^{-1}$. (b) Tafel plots for methanol oxidation on Pt/C and Pt/graphene electrodes.

signal (S) was evaluated in the analyte solution. In both cases, steady-state current resulting during the 120 s is used for calculating the S/N response. In both the cases Pt/graphene displayed a larger S/N ratio (S/N = 5.9) than Pt/C (S/N = 4.16). The larger S/N ratio exhibited by Pt/graphene indicates that the graphene particles are comparatively smaller than the Vulcan employed in this work [47]. The greater S/N ratio exhibited by graphene in this work clearly demonstrates the suitability of employing graphene for methanol oxidation in DMFCs.

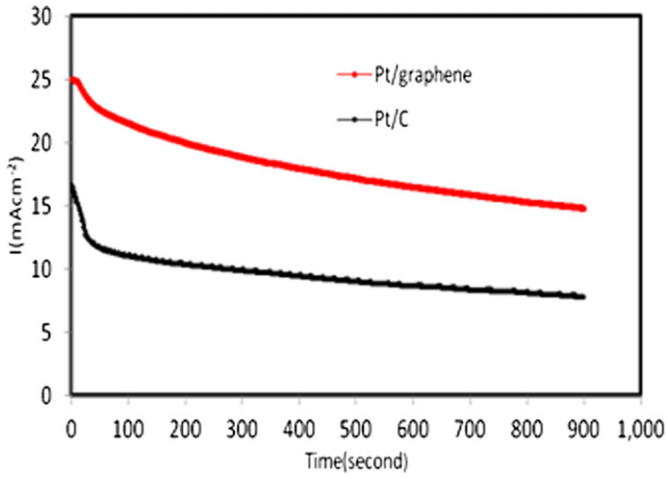


**Fig. 9.** Chronoamperometric response during the oxidation of methanol (1 M) on Pt/graphene and Pt/C electrodes at peak potentials in 0.5 sulfuric acid.

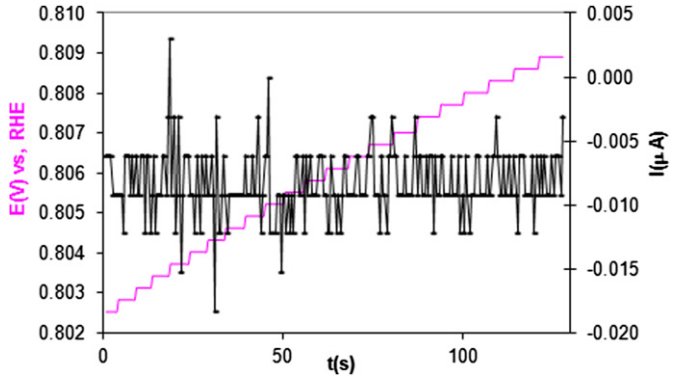


**Fig. 10.** Raw potential and current noise of Pt/graphene electrode in 1 M $CH_3OH$ + 0.5 M $H_2SO_4$.

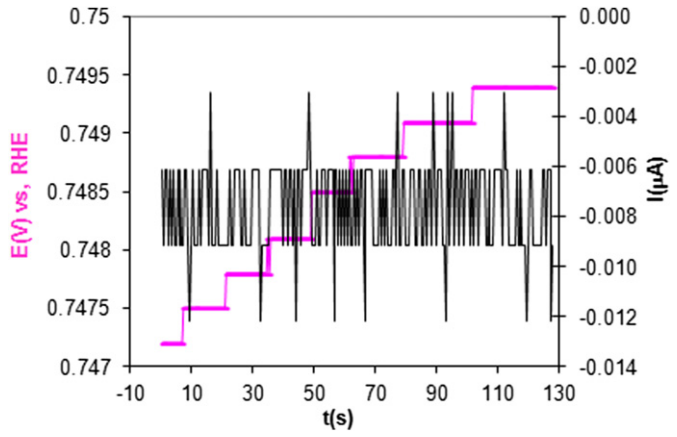


**Fig. 11.** Raw potential and current noise of Pt/C electrode in 1 M $CH_3OH$ + 0.5 M $H_2SO_4$.

## 4. Conclusions

We have developed a unified one-pot electrochemistry method to prepare graphene sheets from the exfoliation graphite electrode. The mechanism of the exfoliation is due to a complex interplay of anodic oxidation of water and anionic intercalation from the ionic liquid.

Pt was reduced by sodium borohydride reduction method with ethylenediaminetetraacetic acid disodium salt (EDTA-2Na) on carbon graphene to use as (DMFC) catalysts. The methanol electroactivity in the Pt/graphene electrocatalyst was found to be 1.81 times higher than in the Pt/C electrode. SEM results confirmed the transparent structure of graphene sheets with few layers. The electrochemical synthesis of graphene nanosheet–nanoparticles composites could be a promising system for methanol oxidation.

## Acknowledgements

This work was supported by the Fuel cell Steering Committee, SANA and Iranian Nano technology initiative council.

## References

[1] A.S. Arico, S. Srinivasan, V. Antonucci, Fuel Cells 1 (2001) 133–161.
[2] K.Y. Chan, J. Ding, J.W. Ren, S.A. Cheng, K.Y. Tsang, Journal of Material Chemistry 14 (2004) 505–516.
[3] V. Mehta, S.J. Cooper, Journal of Power Sources 114 (2003) 32–53.
[4] C. Lamy, A. Lima, V.L. Rhun, C. Coutanceau, J.M. Leger, Journal of Power Sources 105 (2002) 283–296.
[5] A. Hamnett, Catalysis Today 38 (1997) 445–457.

[6] E. Reddington, A. Sapienza, B. Gurau, R. Viswanathan, S. Sarangapani, E.S. Smotkin, T.E. Mallouk, Science 280 (1998) 1735–1737.
[7] P.K. Shen, A.C.C. Tseung, Journal of Electrochemical Society 141 (1994) 3082–3090.
[8] M. Baldauf, W. Preidel, Journal of Power Sources 84 (1999) 161–166.
[9] S. Kim, S.-J. Park, Solid State Ionics 178 (2008) 1915–1921.
[10] H. Liu, C. Song, L. Zhang, J. Zhang, H. Wang, D.P. Wilkinson, Journal of Power Sources 155 (2006) 95–110.
[11] K.S. Novoselov, A.K. Geim, S.V. Morozov, D. Jiang, Y. Zhang, S.V. Dubonos, I.V. Grigorieva, A.A. Firsov, Science 306 (2004) 666–669.
[12] K.S. Novoselov, D. Jiang, F. Schedin, T.J. Booth, V.V. Khotkevich, S.V. Morozov, A.K. Geim, Proceedings of National Academy of Sciences, USA 102 (2005) 10451–10453.
[13] J.D. Fowler, M.J. Allen, V.C. Tung, Y. Yang, R.B. Kaner, B.H. Weiller, ACS Nano 3 (2009) 301–306.
[14] J.T. Robinson, F.K. Perkins, E.S. Snow, Z.Q. Wei, P.E. Sheehan, Nano Letters 8 (2008) 3137–3140.
[15] A. Vollmer, X.L. Feng, X. Wang, L.J. Zhi, K. Mullen, N. Koch, J.P. Rabe, Applied Physics A: Materials Science & Processing 94 (2009) 1–4.
[16] H.A. Becerril, J. Mao, Z. Liu, R.M. Stoltenberg, Z. Bao, Y. Chen, ACS Nano 2 (2008) 463–470.
[17] Q. Wu, Y.i. Xu, Z. Yao, A. Liu, G. ShI, ACS Nano 4 (2010) 1963–1970.
[18] Y. Li, W. Gao, L. Ci, C. Wang, P.M. Ajayan, Carbon 48 (2010) 1124–1130.
[19] Y. Li, L. Tang, J. Li, Electrochemical Communications 11 (2009) 846–849.
[20] S. Bong, Y.-R. Kim, I. Kim, S. Woo, S. Uhm, J. Lee, H. Kim, Electrochemical Communications 12 (2010) 129–131.
[21] D. Lifeng, G.R.R. Sanganna, L. Zhou, C. Michael, H. Shifeng, Carbon 48 (2010) 781–787.
[22] S. Liu, J. Wang, J. Zeng, J. Ou, Z. Li, X. Liu, S. Yang, Journal of Power Sources 195 (2010) 4628–4633.
[23] S.M. Choi, M.H. Seo, H.J. Kim, W.B. Kim, Carbon 49 (2011) 904–909.
[24] N. Jha, R.I. Jafri, N. Rajalakshmi, S. Ramaprabhu, International Journal of Hydrogen Energy 36 (2011) 7284–7290.
[25] Y. Xin, J.-G. Liu, Y. Zhou, W. Liu, J. Gao, Y. Xie, Y. Yin, Z. Zou, Journal of Power Sources 196 (2011) 1012–1018.
[26] Y. Zhao, L. Zhan, J. Tian, S. Nie, Z. Ning, Electrochimica Acta 56 (2011) 1967–1972.
[27] S. Gilje, S. Han, M.S. Wang, K.L. Wang, R.B. Kaner, Nano Letters 7 (2007) 3394–3398.
[28] J. Lu, J.-x. Yang, J. Wang, A. Lim, S. Wang, K.P. Loh, ACS Nano 3 (2009) 2367–2375.
[29] D. Wan, S. Yuan, G.L. Li, K.G. Neoh, E.T. Kang, ACS Applied Materials and Interfaces 2 (2010) 3083–3091.
[30] Y. Wang, Y. Shao, D.W. Matson, J. Li, Y. Lin, ACS Nano 4 (2010) 1790–1798.
[31] P.V. Kamat, The Journal of Physical Chemistry Letters 1 (2010) 520–527.
[32] S. Zhang, Y. Shao, H. Liao, J. Liu, I.A. Aksay, G. Yin, Y. Lin, Chemistry of Materials 23 (2011) 1079.
[33] S. Wang, S.P. Jiang, X. Wang, Electrochimica Acta 56 (2011) 3338–3344.
[34] H. Gharibi, K. Kakaei, M. Zhiani, Journal of Physical Chemistry C 114 (2010) 5233–5240.
[35] C.C. Chien, K.T. Jeng, Materials Chemistry and Physics 99 (2006) 80–87.
[36] J.J. Niu, J.N. Wang, Electrochimica Acta 53 (2008) 8058–8063.
[37] S. Stankovich, D.A. Dikin, G.H.B. Dommett, K.M. Kohlhaas, E.J. Zimney, E.A. Stach, Nature 442 (2006) 282–286.
[38] G. Eda, G. Fanchini, M. Chhowalla, Nature Nanotechnology 3 (2008) 270–274.
[39] H. Gharibi, K. Kakaei, M. Zhiani, M. Mohammadi Taghiabadi, International Journal of Hydrogen Energy 36 (2011) 13,301–13,309.
[40] A. Pozio, M.D. Francesco, A. Cemmi, F. Cardellini, L. Giorgi, Journal of Power Sources 105 (2002) 13–19.
[41] Z. Wang, G. Gao, H. Zhu, Z. Sun, H. Liu, X. Zhao, International Journal of Hydrogen Energy 34 (2009) 9334–9340.
[42] B.K. Jena, C.R. Raj, Langmuir 23 (2007) 4064–4070.
[43] C. Wang, M. Waje, X. Wang, J.M. Tang, C. Haddon, Y. Yan, Nano Letters 4 (2004) 345–348.
[44] A. Velázquez-Palenzuela, F. Centellas, J.A. Garrido, C. Arias, R.M. Rodríguez, E. Brillas, P.-L. Cabot, Journal of Power Sources 196 (2011) 3503–3512.
[45] G. Tremiliosi-Filho, H. Kim, W. Chrzanowski, A. Wieckowski, B. Grzybowska, P. Kulesza, Journal of Electroanalytical Chemistry 467 (1999) 143–156.
[46] H.A. Gasteiger, N. Markovic, P.N. Ross, E.J. Cairns, Journal of Electrochemical Society 141 (1994) 1975–1980.
[47] S. Alwarappan, A. Erdem, C. Liu, C.-Z. Li, Journal of Physical Chemistry C 113 (2009) 8853–8857.
[48] J.T. Long, S.G. Weber, Analytical Chemistry 60 (1988) 2309–2311.
[49] F.H. Estupiñán-López, F. Almeraya-Calderón, R.G.B. Margulis, M.A.B. Zamora, A. Martínez-Villafañe, J.U. Ch, C. Gaona-Tiburcio, International Journal of Electrochemical Sciences 6 (2011) 1785–1796.
[50] M.G. Sung, H. Lee, K. Heo, K.-E. Byun, T. Kim, D.H. Seo, S. Seo, S. Hong, ACS Nano 5 (2011) 8620–8628.